Investigation of gasoline containing GTL naphtha in a spark ignition engine at full load conditions

Wang, C., Chahal, J., Janssen, A., Cracknell, R. & Xu, H.

DOI 10.1016/j.fuel.2017.01.042
ISSN 1873-7153

Publisher: Elsevier

Investigation of Gasoline Containing GTL Naphtha in a Spark Ignition Engine at Full Load Conditions

Authors: Chongming Wang[1,3], Jasprit Chahal[1], Andreas Janssen[1], Roger Cracknell[2], Hongming Xu[3]

[1.] Shell Global Solutions (Germany), Germany; [2.] Shell Global Solutions (UK), UK; [3.] University of Birmingham, UK;

Abstract

Gas-to-liquid (GTL) naphtha can be used as a gasoline blend component, and the challenge of its low octane rating is solved by using ethanol as an octane booster. However, currently there is little knowledge available about the performance of gasolines containing GTL naphtha in spark ignition engines. The objective of this work is to assess full load performance of gasoline fuels containing GTL naphtha in a modern spark ignition engine. In this study, four new gasoline fuels containing up to 23.5 vol.% GTL naphtha, and a standard EN228 gasoline fuel (reference fuel) were tested. These new gasoline fuels all had similar octane rating with that of the standard EN228 gasoline fuel. The experiments were conducted in an AVL single cylinder spark ignition research engine under full load conditions in the engine speed range of 1000-4500 rpm. Two modern engine configurations, a boosted direct injection (DI) and a port fuel injection (PFI), were used. A comprehensive thermodynamic analysis was carried out to correlate experiment data with fuel properties. The results show that, at the full load operating conditions the combustion characteristics and emissions of those gasoline fuels containing GTL naphtha were comparable to those of the standard EN228 gasoline fuel. Volumetric fuel consumption of fuels with high GTL naphtha content was higher due to the need of adding more ethanol to offset the reduced octane rating caused by GTL naphtha. Results also indicate that, compared to the conventional compliant E228 gasoline fuel, lower particulate emissions were observed in gasoline fuels containing up to 15.4 vol.% GTL naphtha.

Keywords: GTL Naphtha; Gasoline; Blend Component; Spark Ignition

1. INTRODUCTION

The gas-to-liquid (GTL) Fischer Tropsch technology converts natural gas into high-quality liquid hydrocarbon products that would otherwise be made from crude oil [1]; therefore, the GTL technology reduces the dependence on crude oil. GTL products include GTL gasoil, GTL naphtha, GTL kerosene, GTL normal paraffin and GTL base oils [2].

GTL gasoil is currently used in compression ignition engines; therefore, it is also named as GTL diesel [3]. It consists almost exclusively of straight chain normal-paraffins and branched iso-paraffins; therefore, it has lower concentrations of aromatics, poly-aromatics, olefins. Additionally sulphur and nitrogen are lower than a conventional diesel. The low poly-aromatic content of GTL diesel are beneficial to reduce particulate matter (PM) emissions from diesel engines, providing more flexibility of controlling oxides of nitrogen (NOx) emissions by using exhaust gas recirculation (EGR) without compromising smoke emissions. The low sulphur content leads to a low tendency of deteriorating after treatment catalysts. The high cetane rating of GTL diesel is beneficial for the diesel engine combustion [3].

A wide range of research has been conducted on the combustion characteristics and emissions of GTL diesel using single cylinder and multi-cylinder engines, optical engines, and commercial vehicles under standard testing cycles, and real world driving conditions [4-14]. It has proved that the GTL diesel has the potential to deliver comparable engine performance and lower emissions to a conventional diesel without major engine hardware modifications. For example, Nishiumi and Clark et al. tested a GTL diesel on an in-line four cylinder diesel engines with a modified combustion chamber, a redesigned injection pattern, and a new EGR calibration [5]. Test results demonstrated that the combination of the GTL diesel and modified engine had the potential to reduce emissions whilst keeping the features of diesel engines such as low CO_2 emissions. The after treatment system for near-

zero sulphur GTL diesel fuel was optimised, resulting in improved the catalyst durability performance and higher NOx reduction efficiency because the catalyst can be designed to improve a low temperature activity and heat resistance. Clark et al. investigated effects of GTL diesel properties on diesel combustion [7]. Six GTL diesel fuels were formulated with various distillation characteristics and cetane number, and their spray behaviour, mixing characteristics, combustion and emissions were studied. Results showed that fuels with low distillation temperature and a high cetane rating led to reduction of hydrocarbon and particulate emissions, and combustion noise, which was explained by enhanced air/fuel mixing of the lighter fuel, high ignitability and short ignition delay.

Apart from engine combustion characteristics and emissions of GTL diesel fuels, some studies have been carried out focusing on the impact of GTL diesel fuels on fuel injection system. Lacey and Stevenson et al. evaluated the long-term performance of GTL diesel fuels in advanced common rail fuel injection systems [15]. Tests on engine testing cell, and electrically driven common rail pump hydraulic rig tests showed that the performance of GTL diesel was at least comparable to conventional hydrocarbon fuels and superior in a number of areas, and no deposits were produced on fuel injection system components even under severe operating conditions.

GTL naphtha, one of the products from the GTL process, mainly contains a light fraction of C4 to C11 hydrocarbons with a high proportion of straight chain paraffins. GTL naphtha is an alternative high-quality feedstock for plastics [2]. As a synthetic product, GTL naphtha has a consistent quality and contains near-zero sulphur and heavy metals, which makes it cleaner [2].

Searching for potential direct uses of GTL naphtha is of interest. Historically, it has not commercially been used in vehicles, because GTL naphtha has a low octane rating, making it unsuitable to be directly blended into conventional gasoline and be used in SI engines. The introduction of bio-ethanol as a blending component has made the octane rating of GTL naphtha a less limiting factor because ethanol has a high octane rating. However, currently there is little knowledge available about the performance of gasolines containing GTL naphtha in spark ignition engines.

In this study, four gasoline fuels containing up to 23.5 vol.% GTL naphtha, three of which were close to being EN228 compliant, were tested in an AVL state-of-art single cylinder gasoline research engine. A standard EN228 gasoline fuel was used as a benchmark for comparison. Two modern engine configurations, a boosted direct injection (DI) and a port fuel injection (PFI), were selected. The tests were conducted under full load condition in the engine speed range of 1000-4500 rpm. The focus was on the assessment of full load combustion characteristics and emissions of these new gasoline fuels with GTL naphtha. A comprehensive thermodynamic analysis was carried out to correlate engine data with fuel properties.

2. EXPERIMENTAL SYSTEMS AND METHODS

2.1. ENGINE AND INSTRUMENTATION

The engine used in this study is an AVL single cylinder 4-stroke spark ignition research engine, of which the specifications and setup are listed and presented in Table 1 and Figure 1, respectively. Its combustion system features a 4-valve pent roof cylinder head equipped with variable valve timing (VVT) systems for both intake and exhaust valves. The cylinder head is equipped with a central-mounted outward opening high pressure piezo direct injector, and a low pressure PFI. The PFI injector is located in the intake manifold pointing towards intake valves. The spark plug is located at the centre of the combustion chamber slightly tilting towards the exhaust side.

The engine is coupled to an electric dynamometer, which is able to maintain the engine at a constant speed (± 1 rpm) regardless of engine power outputs. Intake and exhaust plenums with a capacity of approximately 3 L and 50 L are used to stabilize the intake and exhaust flow for this single cylinder engine. The engine is controlled through an IAV FI2RE management system. An AVL Indicom system with inputs from sensors such as high resolution in-cylinder, intake and exhaust pressure transducers is used for real time combustion indication and analysis. A high resolution crankshaft encoder (0.1 ℃AD) is used for engine knocking analysis. A Siemens CATs system is used

for signal acquisition and recording, and it communicates with the IAV FI2RE management system and the AVL Indicom. It is also used for controlling air, fuel, coolant and oil conditioning units, and emission measurement equipment.

A Kistler pressure transducer used for cylinder pressure measurement is installed in a sleeve on the intake and exhaust bridge. Cylinder pressure is collected via a charge amplifier (ETAS ES630.1) with a resolution of 0.1 °CA between 30 °CAD before top dead centre (BTDC) and 70 °CAD after top dead centre (ATDC), and a resolution of 1 °CA in the rest of the cycle. Some key temperature and pressure measurement points are briefly labelled as 'T' and 'P', respectively, and are shown in Figure 1. The shaft encoder used in this study is a 365C Angle Encoder Set provided by AVL. It is a high precision sensor for angle-related measurements mainly for indicating purposes.

An external air handling device, capable of delivering up to 0.3 MPa boosted air, is used in this study. Air is firstly filtered and dried, and then is delivered to a conditioning system with a capacity of approximately 200 L, in which its pressure and temperature can be precisely close-loop controlled. Temperatures of fuel, coolant and oil are also precisely controlled by individual AVL conditioning units.

Fuel consumptions are measured by an AVL fuel mass flow meter. Gaseous emissions are measured using a Horiba MEXA-7100D gas analyser. Particulate mass (PM) and particulate number (PN) emissions are measured using an AVL Micro Soot Sensor and an AVL 489 Advanced Particle Counter, respectively. The exhaust is sampled 5 m downstream of the exhaust ports, just after the exhaust back pressure regulator via heated lines (maintained at 464 K) to the analysers.

2.2. FUELS

Table 2 lists physiochemical properties of fuels (additive free) used in this study. Fuel A (reference fuel) was a typical EN228 compliant gasoline, and Fuels B-E had similar octane rating with Fuel A. Fuel B contained 7.3 vol.% GTL naphtha but no ethanol. Fuels C-E were blends of various

refinery streams, GTL naphtha (12.8 vol.% - 24 vol.%), and ethanol (5 vol.% - 20 vol.%). Fuels B-D were almost EN228 compliant; however Fuel E had an oxygen content of 7.2 wt.%, which exceeded the EN228 upper limit of 3.7 wt.%.

2.3. ENGINE CONFIGURATIONS AND EXPERIMENTAL PROTOCOL

DI and PFI engine configurations were selected for fuels' performance assessment. In both engine configurations, the compression ratio was 9.5:1. Table 3 lists the test protocol. Full power tests with engine speeds ranging from 1000-4500 rpm were tested under defined intake manifold pressure. Under the compression ratio of 9.5:1, the maximum intake manifold pressure tested in this study was 0.2 MPa. The parameters, such as intake and exhaust valve timing, and injection strategy (see Table 3), were optimised for Fuel A and used for all other fuels. In this study, all the fuels were designed with similar octane ratings, it is expected that the optimised spark timing for all fuels would be similar; therefore, it was decided that the optimised spark timing map for Fuel A was used for all fuels. Additionally, comparing combustion characteristics under the same spark timing maps for all fuels make it possible to evaluate the burning speed of these fuels.

2.4. DATA PROCESSING

The combustion parameters such as IMEP, heat release rate, combustion phase and mass fraction burn (MFB) profiles were calculated by the AVL IndiCom and the AVL Concerto software. In order to convert the particulate number emission from the unit of #/cm^3 to #/kWh, the following equation was used.

$$[PN] = [cc_{PN}] * \frac{1}{\rho_{exh}} * \frac{\dot{m}_{fuel} + \dot{m}_{air}}{Power} * 10^6$$

where $[PN]$ and $[cc_{PN}]$ is the particulate number emission expressed in the units of #/kWh and #/cm^3, respectively. ρ_{exh} is the density of exhaust in the unit of kg/m^3, and the temperature and pressure used for exhaust density calculation was 273 K and 0.1013 MPa, respectively. The reason for using this temperature and pressure is because the AVL particulate counter and AVL soot sensor calculated the mass- and number- concentration under this condition.

In order to convert the particulate mass emission from the unit of mg/m^3 to mg/kWh, the following equation was used.

$$[PM] = [cc_{PM}] * \frac{1}{\rho_{exh}} * \frac{\dot{m}_{fuel} + \dot{m}_{air}}{Power}$$

where $[PM]$ and $[cc_{PM}]$ is the particulate mass emission expressed in the units of mg/kWh and mg/m^3, respectively.

Engine knocking related parameters, such as pressure oscillation and knocking frequency distributions were calculated by using an in-house Matlab code. In-cylinder pressure oscillation for each engine cycle was obtained by filtering the raw in-cylinder pressure data by a brand-pass filter (3-30 kHz). Knock intensity in this study is defined as the maximum amplitude of the filtered and rectified in-cylinder pressure oscillation (MAPO). Frequency distribution of the in-cylinder pressure was obtained by using the Fast Fourier Transform (FFT) mathematic function. Knock onset is defined at the first crank angle position where a rapid raise of pressure rise occurred in the pressure oscillation profile.

3. RESULTS AND DISCUSSION

Results of combustion characteristics and fuel economy are provided in this section because they are significantly important for the understanding of the impact of fuels on internal combustion engines. In the spark ignition engines, key combustion parameters include combustion delay, combustion

duration, in-cylinder pressure profile and mass fraction profile, which reveal the potential and feasibility of burning specific fuels in SI engines.

3.1. COMBUSTION CHARACTERISTICS

Figure 2 presents the full load IMEP of all the fuels under various engine speeds. Clearly, all the fuels delivered the similar maximum IMEP under both the DI and PFI configurations. This is because under the stoichiometric AFR combustion the calorific values of the fuels mixed with 1 kilogram of air are in a narrow range of 2.88-2.91 MJ/kg (see Table 2). Compared to the PFI configuration, the DI configuration led to higher IMEP, which was due to cooling effect of direct injection and more advanced spark timing (see Table 3). For the DI engine configuration at the engine speeds of 3500 and 4500 rpm, fuel enrichment was required to limit exhaust temperatures. The same was true for the PFI engine configuration at the engine speed of 3500 rpm. The IMEP at the engine speed of 1000 rpm was significantly lower than that at the other engine speeds mainly due to the lower boost pressure. For both the DI and PFI configurations, the IMEP at engine speeds of 3500 and 4500 rpm were higher than that of 1800 rpm even though the boost pressure settings were the same, because at higher engine speeds spark timings were more advanced (see Table 3).

Figure 3 presents the knock intensities of all the fuels at full load under various engine speeds. The knock intensity shown in this figure is the averaged MAPO over two-minute measurements. For each engine cycle, in-cylinder pressure oscillation signal was obtained by filtered the in-cylinder pressure by a band filter (3-30 kHz), and then it was rectified. The knock intensity for a given engine cycle is the maximum amplitude of pressure oscillation (MAPO) for that cycle. In the study of engine efficiency improvement through engine design and high octane fuel, Leach et al. [16] defined the MAPO upper limit (engine speed dependent) at 0.09-0.55 MPa over the engine speed of 1000-6000 rpm, which was approximately 0.1 MPa/1000 rpm. The reason that knock upper limits depend on engine speed is because the engine is more tolerated to knocking at higher engine speed due to less time available for auto-ignition.

196 The knock upper limits used in [16] were also tested in this study. It was found that the engine was
197 operated safely under these knock upper limits, and further increasing the upper limits led to clear
198 increased audible noises. However, the problem of using the MAPO as a parameter is that it varies
199 from cycle-to-cycle significantly, which makes it difficult to control engine knocking. It was found
200 that the averaged MAPO over 50 cycles was a better parameter for monitoring and controlling engine
201 knocking. Obviously, the averaged MAPO over 50 cycles was much lower than the maximum MAPO
202 over the 50 cycles. In this study, the same spark timing calibration optimized for Fuel A was used for
203 all other fuels (see Table 3). The anti-knock ability of fuel is largely dependent on its octane rating and
204 the cooling effect if the direct injection is used. For pure ethanol, some research evidence shows that
205 its cooling effect in DI engines is equivalent up to 18 octane units [17, 18]. In this study, larger
206 differences in knock intensity were observed at the engine speed of 1000 rpm than the other engine
207 speeds, where Fuel A with the least heat of vaporization had the highest knock intensity whilst Fuel E
208 with the highest heat of vaporization had the lowest knock intensity. In SI engines, knocking occurs
209 when auto-ignition happens to end-gas before the normal propagation of flame triggered by ignition.
210 Engine knocking tends to happen in low engine speed and high load regions [19-21].

211 Figure 4 shows the pressure oscillations of Fuels A and Fuel E at the engine speed of 1000 rpm,
212 and full load condition. In Figure 4, the pressure oscillations for Fuel E have offset by +0.05 MPa. The
213 reason why these two fuels were selected for pressure oscillation analysis was because they were at the
214 two ends of the knocking resistant spectrum among all the fuels. The data presented in Figure 4 was
215 not averaged results from the 200 cycles recorded for each test point, but it was taken from a cycle that
216 had a MAPO closest to the averaged MAPO. The knock onset is a parameter for distinguishing pre-
217 ignition and knocking, and also is used for calculating the knocking delay after the event of ignition. If
218 the knock onset is earlier than ignition, this cycle is defined as a pre-ignition cycle rather than a
219 knocking cycle. In both the DI (Figure 4(a)) and PFI (Figure 4(b)) configurations, it is clear that those
220 cycles are knocking cycles. Fuel A experienced higher pressure oscillations and more advanced knock

onset that those of Fuel E. For example, in the PFI configuration, the knock onset for Fuel A and Fuel E were 24.8 °ATDC and 36.4 °ATDC, respectively. It means that the end gas of Fuel A auto-ignited approximately 12 CAD earlier than that of Fuel E. Another phenomenon should be pointed out is that, knocking intensity quickly raised after the knock onset, and it attenuated gradually due to energy losses as the knock wave propagates and bounces within the cylinder liner.

Figure 5 shows knock intensity probability distributions of Fuels A and Fuel E at the engine speed of 1000 rpm and full load condition. The data in Figure 5 are the statistical analysis of a few hundred of cycles. In both the DI (Figure 5 (a)) and PFI (Figure 5 (b)) configurations, it is clear that compared to Fuel A, Fuel E had a higher knocking distribution in the low knocking intensity region (MAPO < 0.01 MPa), and a lower knocking distribution in the high knocking intensity region (MAPO > 0.01 MPa). For both Fuels A and Fuel E, the probability distribution profile was skewed left, and the probability of high-end knocking intensities was relatively lower compared to the low-end knocking intensities.

When engine knock happens, the auto-ignited gas creates a sudden and violent pressure waves/shocks propagating inside the combustion chamber, leading to resonance of engine parts and audible knocking noises. The resonance frequencies are a function of many factors such as the combustion geometric and the wave media. In passenger car engines, a squat cylindrical combustion chamber experiences radial and circumferential resonance modes [22-24]. The axial modes are neglected because the engine knock happens close to the TDC. A simplified wave equation proposed by Draper [20] and used by many other researchers [22-24] are given as follow :

$$f_{(m,n)} = \alpha_{(m,n)} * \frac{\sqrt{\gamma RT}}{\pi * B} = \alpha_{(m,n)} * \frac{c}{\pi * B}$$

where $f_{m,n}$ is the knocking frequency for the m (radial) and n (circumferential) mode; $\alpha_{m,n}$ is the resonance mode factor determined from Bessel functions; γ is the ratio of specific heats; R is the ideal

gas constant; T is the temperature; c is the sound velocity in the combustion chamber; B is the dimension of cylinder bore.

The sound velocity for the burned gas/air and fuel mixture in gasoline engines can be roughly estimated at 950 m/s [25, 26]. The resonance mode factors are 1.84, 3.05, 3.83 and 4.20 when (m, n) are (1, 0), (2, 0), (0, 1) and (3, 0), respectively [22]. The theoretical resonant frequencies for those modes mentioned above are 6.57, 10.89, 13.68 and 15.00 kHz, respectively.

Figure 6 shows the single-side pressure amplitude spectrum distribution of FFT filtered pressure for Fuels A and E at the engine speed of 1000 rpm and full load condition. It can be seen that the pressure amplitudes were much higher at the low frequency region where normal combustion happened. In both the DI and PFI configurations, there was no peak in the spectrum for Fuel E. In the DI configuration, peaks existed at the resonant frequencies of 7, 12.4 and 16.6 kHz for Fuel A, which approximately corresponded to the first radial mode (1, 0), the first circumferential mode (0, 1) and the third radial mode (3, 0). In the PFI configuration, the peak of pressure amplitude spectrum exited at the 7 and 16.6 kHz, which represented the first radial mode (1, 0) and the third radial mode (3, 0). The deviation between experiment and theoretical resonant frequencies are possibly due to the rough estimations of sound velocity.

The speed of sound was recalculated by minimizing the sum of squared residuals between the experiment and theoretical resonant frequencies. The recalculated speed of sound was 939 m/s, which gave the resonant frequencies of 6.7, 14.0 and 15.3 kHz at the first radial mode (1, 0), the first circumferential mode (0, 1), and the third radial mode (3, 0), respectively. The corresponding temperature for this speed of sound was 2211 K. For the PFI and DI configurations, the resonant frequencies at the first radial mode (1, 0) and the third radial mode (3, 0) were the same. This shows that Fuel A started to be auto-ignited at the same temperature (2211 K), regardless of engine configurations.

Figure 7 presents the combustion delays of all the fuels at full load under various engine speeds. The combustion delay is defined as the crank angle intervals between ignition and 5% of MFB. For the DI configuration, the differences in combustion delays were approximately 1 CAD, and the order is: B<A≈C≈D<E, which matched the order of the HoV. Since the spark timing setting of all fuels were kept the same, the in-cylinder temperature difference at the timing of ignition was mostly due to the cooling effect of fuels, and the fuel with a high HoV led to lower temperature, and thus longer combustion delay. For the PFI configuration, the effect of heat of vaporization was less clear because the fuel was injected in the intake port instead of directly in the cylinder.

Figure 8 presents combustion characteristics of all the fuels at full load under various engine speeds. CA5-90 represents the crank angle interval between 5% and 90% of MFB, which is used to describe the combustion duration. For the DI configuration, the differences in combustion durations (CA5-90) between Fuels B to E and Fuel A were limited (less than 1CAD). When combustion durations (CA5-90) were broken down into CA5-50 and CA50-90, more differences in combustion burning rate were observed in the second-half of combustion (CA50-90), which can be explained as the temperature and pressure during the CA50-90 were much higher than those during the CA5-50, and thus differences in burning rate between fuels would be more obvious. Fuel E had relatively long CA5-90, CA5-50 and CA50-90. The possible explanation is that with Fuel E led to more fuel wetting because it has the highest HoV and the lowest energy density. The boiling point of ethanol is relatively lower than the most of hydrocarbon components in the gasoline, and the HoV of ethanol is much higher than gasoline; therefore, heavy hydrocarbons impinged on the cylinder liner/wall were difficult to be vaporized. Additional optical diagnostics in an optical engine can provide evidence for this assumption.

Figure 9 presents the maximum in-cylinder pressure of all the fuels at full load under various engine speeds. For both the engine configurations, the maximum in-cylinder pressure differences between Fuels B to D and Fuel A were limited (< 0.2 MPa). At 1000 rpm engine speed, Fuel E had 0.5

MPa lower maximum in-cylinder pressure than Fuel A, resulting from a longer combustion duration. The difference in the maximum in-cylinder pressure between the DI and PFI configurations were mainly due to different ignition settings.

Figure 10 presents the normalized ISFC of all the fuels at full load under various engine speeds. The 'normalized ISFC' means the ISFC was normalized by the 42 MJ/kg low calorific value in order to eliminate the difference in low calorific values between fuels. Generally, the difference in the normalized ISFC between Fuel A and Fuels B-E were within 2%. At fuel enrichment operating points, including 3500 and 4500 rpm engine speed in the DI configuration, and 3500 rpm in the PFI configuration, the normalized ISFC were significantly lower than those of at 2500 rpm engine speed where no fuel enrichment was required. It is worth to point out that, in this study insufficient repeats (< six repeats) were conducted; therefore, no statistical significance analysis can be provided regarding the fuel consumption data.

3.2. ENGINE OUT EMISSIONS

Figure 11 presents indicated specific gaseous (total HC, CO and NO_x) emissions for all the fuels at full load under the DI and PFI engine configurations. Overall, gaseous emissions of all fuels at full load were comparable.

There was limited difference in the CO emissions of all the fuels. In both engine configurations, fuel enrichment for the purpose of limiting exhaust temperature led to high CO emissions due to the lack of oxygen for complete combustion. Fuel enrichment, on the other hand, led to low NO_x emissions due to reduction in combustion temperature. Interestingly, Fuel E produced slightly higher NO_x emissions than other fuels. The possible reason is that, the low boiling point ethanol (78 ˚C) promoted the vaporization of light and medium hydrocarbons in Fuel E, making it harder for heavy hydrocarbons to evaporate and form combustible mixtures. In addition, more fuel quantity was

injected for Fuel E compared with other fuels due to its low energy density; hence more fuel impingement/wetting would be anticipated. The two points mentioned above could have caused Fuel E have more diffusive combustion near the surface of cylinder liner and piston top. The diffusive combustion potentially encouraged the NOx formulation; therefore, Fuel E produced higher NOx emissions. The reason that Fuel E had higher NOx emission even at the PFI configuration is that the engine was running at full engine load, and the fuel injected (PFI) on the intake valves had very limited time for vaporization especially at high engine speeds, leading to large droplets of fuels directly flow into the cylinder by the force of intake air movements, which caused cylinder wall wetting, and diffusive combustions. Fuels B to D consistently produced slightly less HC emissions than Fuel A in both engine configurations. In the DI engine configuration, Fuel E led to slightly higher (2%-10%) HC emissions than Fuel A, this also confirmed that Fuel A experienced more diffusive combustion due to more fuel impingement. It is worthy to point out that a flame ionization detector (FID) from Horiba MEXA-7100D was used for the measurement of HC emissions. The FID is widely used for the analysis of THC. However, this type of detector is subjected to reduced sensitivity to oxygenated hydrocarbon, as reported Wallner [27] and Price et al [28]. For example, the FID's response factor towards formaldehyde and acetaldehyde are only 0.2 and 0.6 respectively whilst toluene is 1. Therefore, the HC emissions reported in this study were underestimated for fuels containing ethanol.

Figure 12 presents particulate emissions for all fuels at full load under the DI and PFI engine configurations. In both engine configurations, Fuels A consistently produced higher PN and PM emission than Fuels B to D. Fuel E produced similar PN and PM emissions to Fuel A possibly because of more diffusive combustion mentioned above. There are several publications which reported the increase of particulate emissions for ethanol blends [29-32]. It is suggested that by optimizing the combustion chamber and injection spray, it is possible that fuel impingement can be avoided or at least reduced so that ethanol blends lead to a benefit of reduced particulate emissions [33-35].

4. CONCLUSIONS

In this study, four gasoline fuels containing up to 23.5 vol.% GTL naphtha, three of which contained up to 20 vol.% ethanol contents, were tested in an AVL single cylinder gasoline research engine. The results were compared with an EN228 compliant gasoline. The tests were conducted under full load conditions in the engine speed range of 1000-4500 rpm. The following are the conclusions drawn from this study:

1. The formulated gasoline fuels were successfully used in a modern gasoline engine without any hardware modifications. In both DI and PFI engine configurations and full load conditions, these formulated gasoline fuels led to comparable combustion characteristics and full power output to conventional gasoline.
2. At the full load conditions, less than 2% differences in the normalized ISFC were observed between the formulated gasoline fuels and the conventional gasoline.
3. Gaseous emissions of the formulated gasoline fuels were similar to, if not lower than that of conventional gasoline. Therefore, it is suggested that, there needs to be no further modifications to exhaust three-way catalysts if these gasoline fuels were used in conventional SI engines.
4. Compared to the conventional gasoline, lower particulate emissions were observed in gasoline fuels containing up to 15.4 vol.% GTL naphtha and 10 vol.% ethanol.

It should be noted that the engine performance and emissions of these formulated gasoline fuels were collectively influenced by GTL naphtha, ethanol and other hydrocarbons. Further investigation is required to understand the GTL naphtha's impact on combustion and emissions in internal combustion engines. In this study, due to the limited amount of GTL naphtha available and the time constrain, less

than six repeats were conducted for each fuel; therefore, no robust statistical significance analysis can be provided. Additional repeat tests on this engine and further tests on a wider range of engines/vehicles would be required to generalize the validity of these findings.

ACKNOWLEDGMENT

This work was conducted at the Shell Technology Centre Hamburg. Dr. Chongming Wang was financially supported by the European Commission through the Marie Curie Program (PIAP-GA-2013-610897 GENFUEL). Authors at the University of Birmingham and Shell Global Solutions (Germany) would like to thank Jakob Beutelspacher and Jan-Henrik Gross for their supports in fuel blending and engine testing.

Tables

Table 1: Engine specifications

Parameters	Details
Combusiton system	4-valve pent roof spark ignition
Displacement/bore/stroke	454 cm^3/82 mm/86 mm
Compression ratio	7-14 (variable)
Injection/ Injection pressure	Direct piezo injector/up to 20 MPa; PFI injection/0.45 MPa
Ignition system	Ignition coil
Engine management system	IAV GmbH – FI2RE
Maximum boost pressure*	0.3 MPa
Maximum engine speed	6400 rpm

* The maximum boost pressuer the engine can take differs, largely depending on the engine compression ratio. The maximum boost pressure (0.3 MPa) stated in this table is for compression ratio of approximately 7.5:1.

Table 2: Fuel properties

Fuel	Unit	A	B	C	D	E	EN228
GTL Naphtha	vol.%	0	7.3	11.4	15.4	23.5	
Paraffins	Vol.%	47.2	47.9	46.4	52.4	43.4	
Olefins	Vol.%	10.1	11.5	8.8	9.0	0.3	18 max.
Aromatics	Vol.%	26.0	35.22	34.9	25.6	33.0	35 max.
Ethanol	vol.%	4.7	0	5.0	10.0	20.0	10 max.
Oxygen Content	wt.%	2.3	0	1.6	3.1	7.2	3.7 max.
Density @ 15 ℃	kg/m^3	743	749	755	740	767	720-775
RON		95.3	96.0	95.8	96.1	96.2	95 min.
MON		85.2	85.6	84.5	86.1	86.1	85 min.
Stoichiometric AFR		14.17	14.47	14.15	14.09	14.53	
LHV	MJ/kg	40.94	41.97	41.18	40.57	38.17	
LHV	MJ/L	32.55	33.47	33.15	32.32	31.37	
Vapour pressure	kPa	57.8	54.6	56.3	55.3	50.2	45-60
Heat of Vaporization	kJ/kg	394	372	401	424	488	
LHV	MJ/kg_air at stoic.)	2.89	2.90	2.91	2.88	2.89	
HoV	kJ per MJ energy input	9.62	8.86	9.74	10.45	12.78	
Estimated Laminar flame speed*	m/s	0.6944	0.6862	0.6957	0.7049	0.7251	

*The laminar flame speed was estimated under the condition of 1.1 air/fuel equvilaence ratio, 0.3 MPa and 177ºC initial temperature and pressure. The estimation was done by a Shell's internal model using laminar flame speed data base containing a large amount of commen hydrocarbons in gasoline.

Table 3: Full load test protocol

Engine configuration	Engine Speed	Intake manifold pressure	λ	Intake valve open/close timing @ 1mm valve lift	Exhaust valve open/close timing @ 1mm valve lift	Injection timing	Intake Tem.	Ignition	Exhaust back pressure
	rpm	MPa		°ATDC	°ATDC	°ATDC	°C	°ATDC	MPa
DI	1000	0.16	1	7.8/199.1	-229.4/-18.0	-325; -285; -245; -205; -165	38±2	2	0.16
	1800	0.20	1	17.8/209.1	-214.4/-3.0			2	0.20
	2500	0.20	1	22.8/214.1	-214.4/-3.0			-3	0.20
	3500	0.20	0.85	12.8/204.1	-214.4/-3.0			-4	0.20
	4500	0.20	0.8	2.8/194.2	-214.4/-3.0			-7	0.20
PFI	1000	0.16	1	-7.2/184.2	-209.4/2.0	-492	38±2	9	0.16
	1800	0.20	1	17.8/209.1	-219.4 /8.0	-620		4	0.20
	2500	0.20	1	17.8/209.1	-219.4 /8.0	-679		-1.5	0.20
	3500	0.20	0.85	22.8/214.1	-219.4 /8.0	-865		-2.5	0.20

Figures

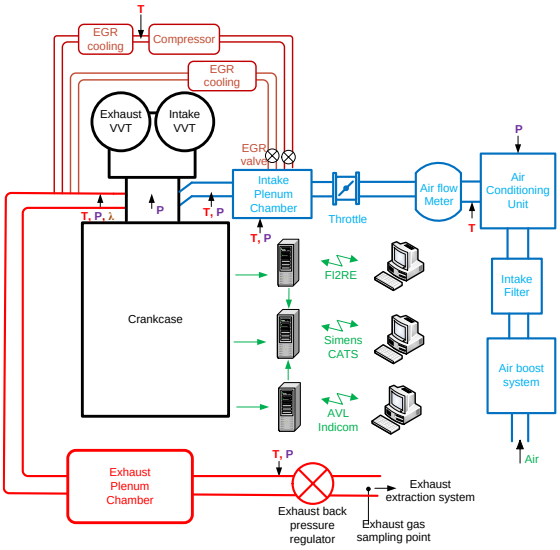

Figure 1: Engine setup

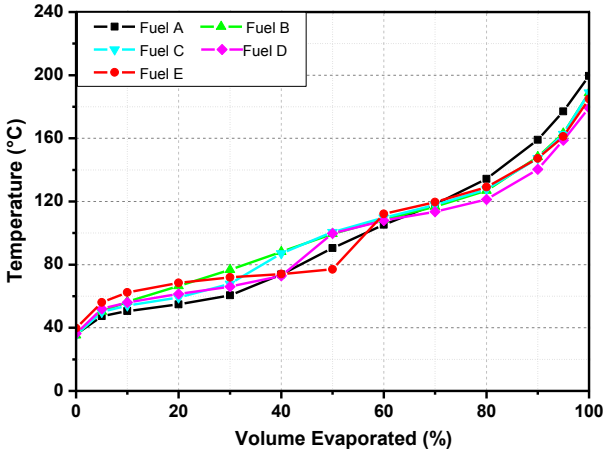

Ci: Distillation profiles for all fuels

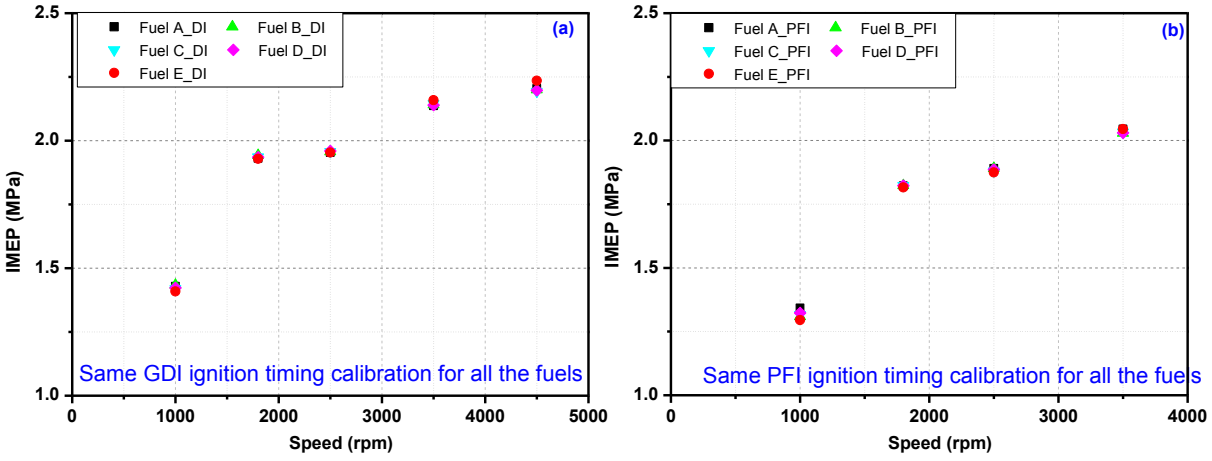

Figure 2: IMEP of all fuels at full load: (a) DI configuration; (b) PFI configuration

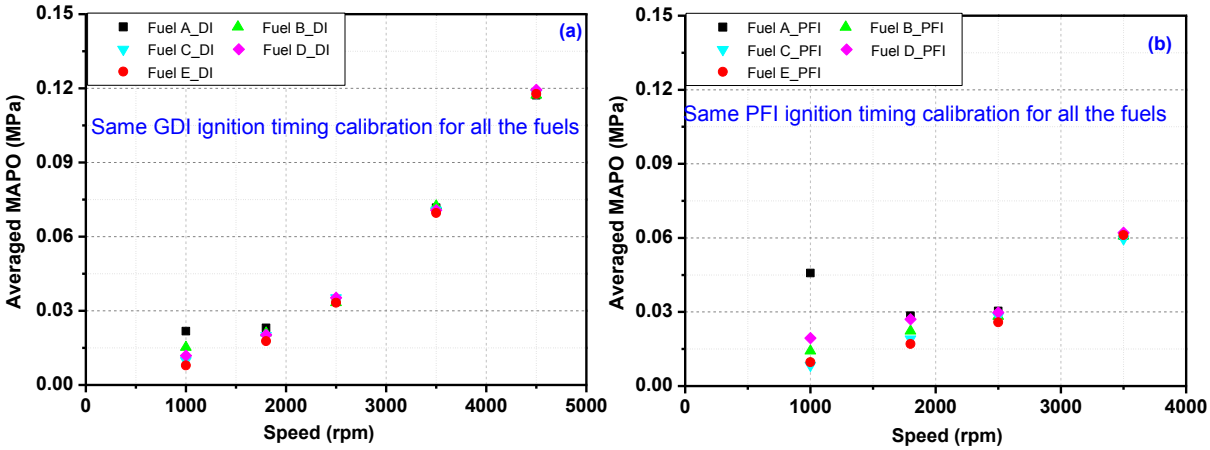

Figure 3: Knock intensities of all fuels at full load: (a) DI configuration; (b) PFI configuration

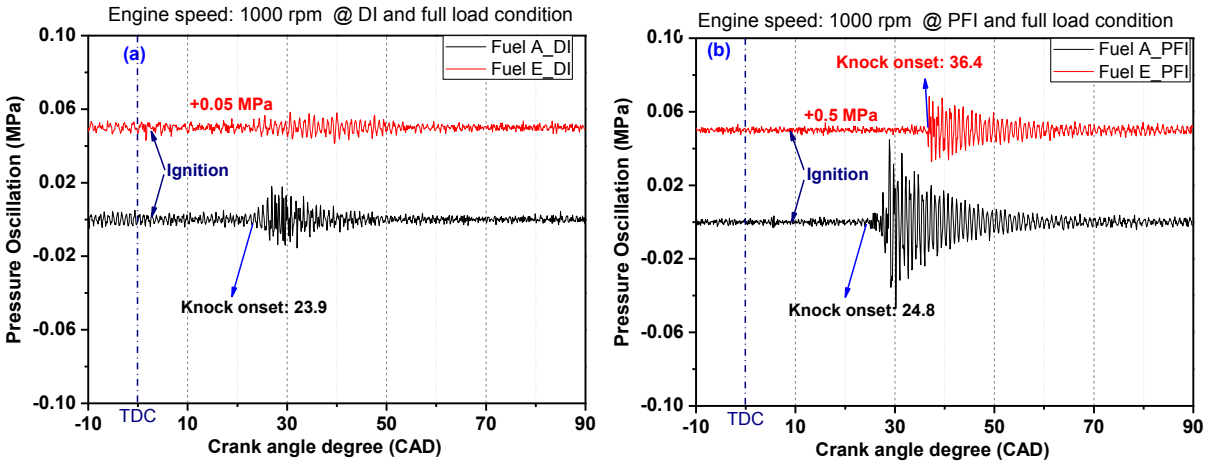

Figure 4: Pressure oscillation for Fuel A and E at 1000 rpm engine speed and full load condition: (a) DI configuration; (b) PFI configuration

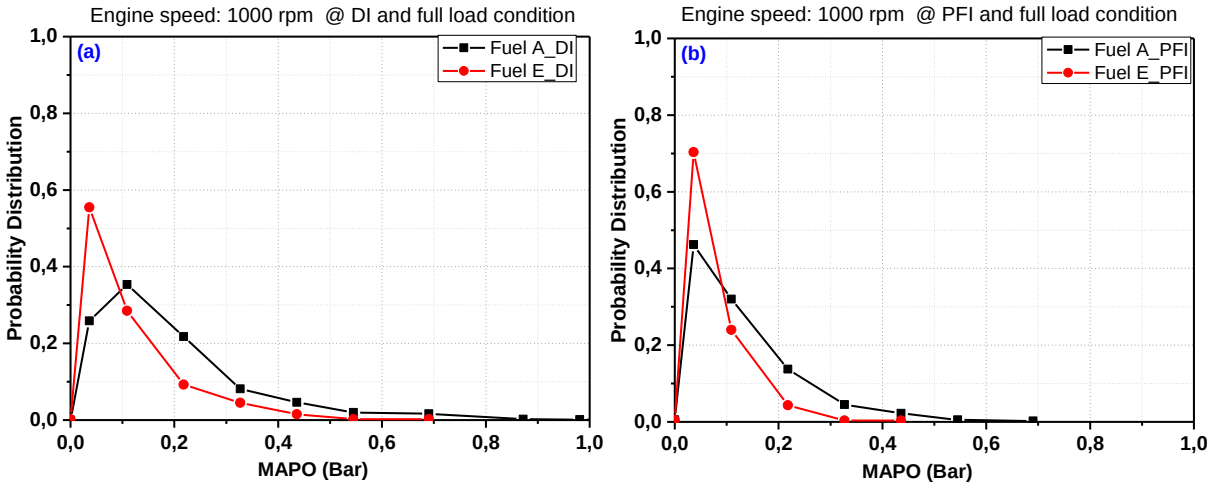

Figure 5: MAPO probability distributions for Fuel A and E at 1000 rpm engine speed and full load condition: (a) DI configuration; (b) PFI configuration

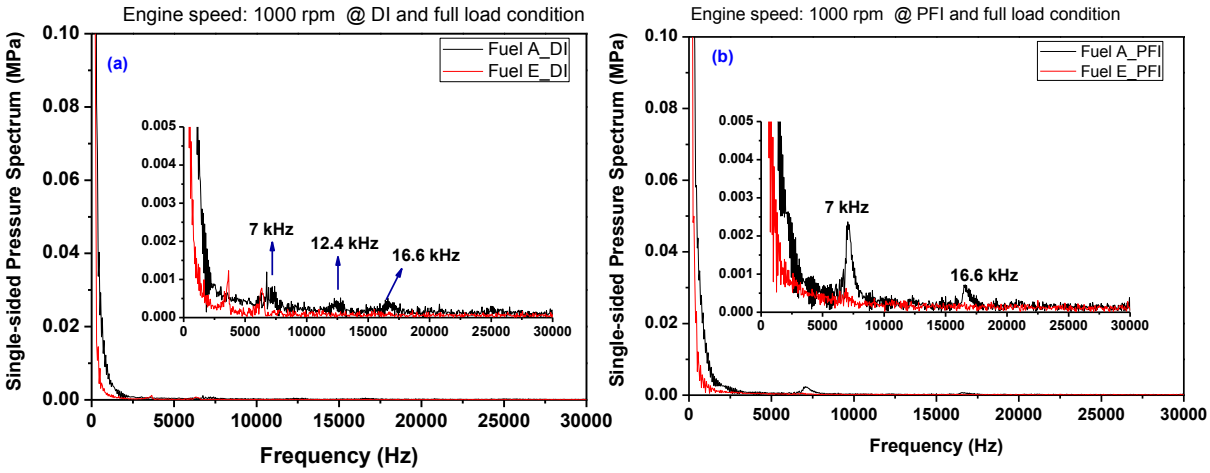

Figure 6: Single-side pressure spectrums of FFT filtered pressure traces for Fuel A and E at 1000 rpm engine speed and full load condition: (a) DI configuration; (b) PFI configuration

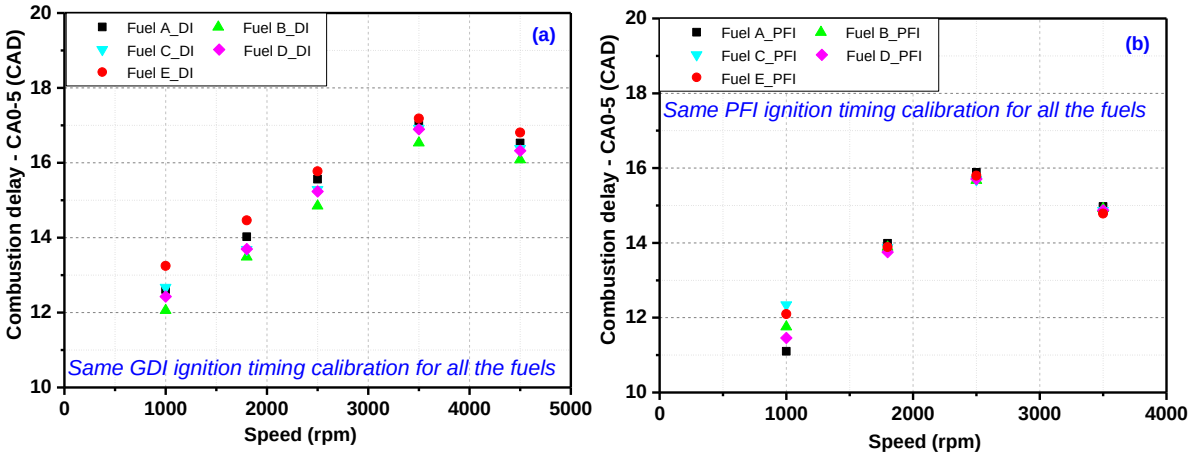

Figure 7: Combustion delay of all fuels at full load: (a) DI configuration; (b) PFI configuration

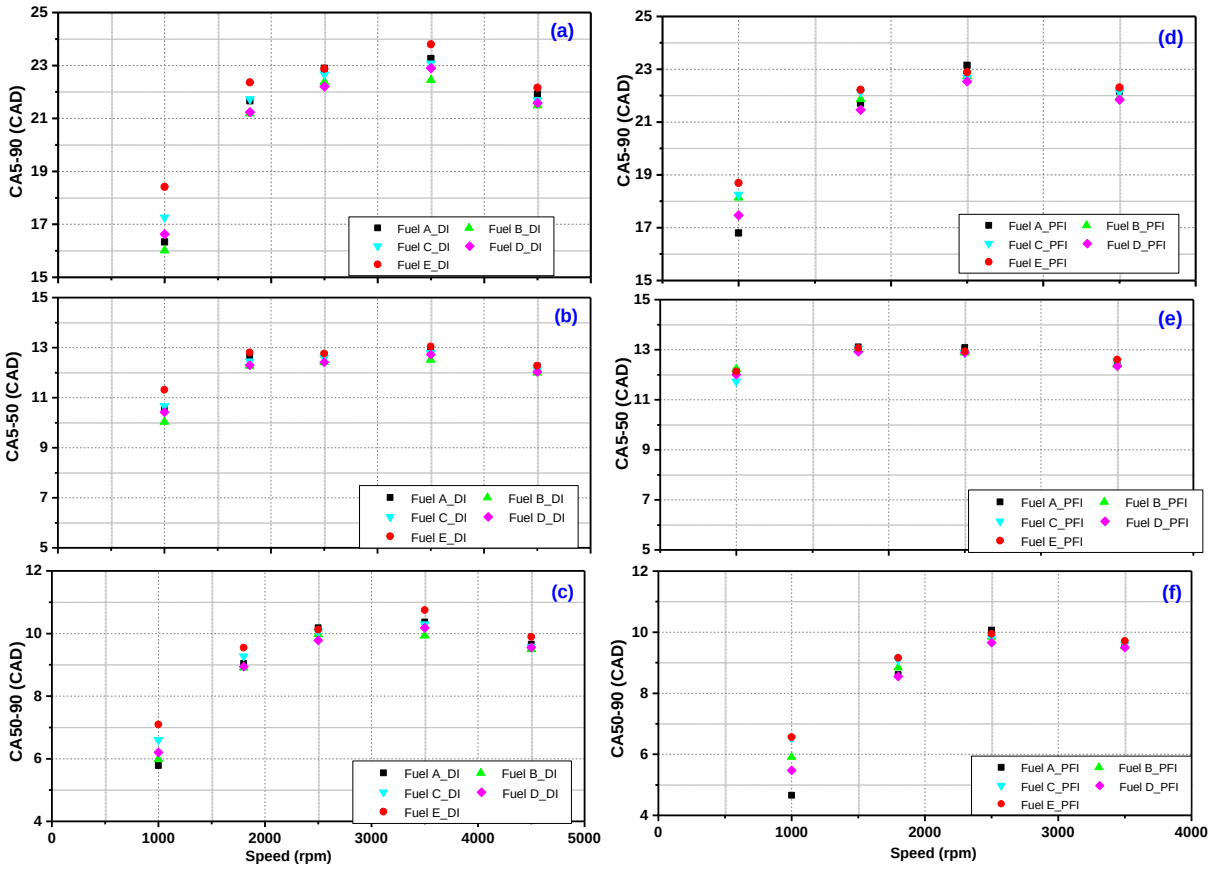

Figure 8: Combustion characteristics of all fuels at full load: (a, b and c) DI configuration; (d, e and f) PFI configuration

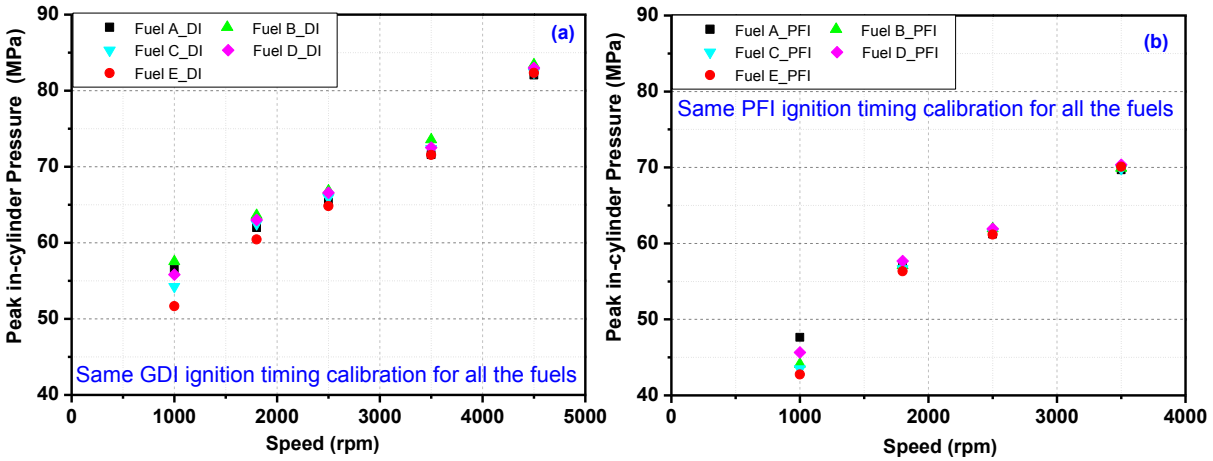

Figure 9: Maximum in-cylinder pressure of all fuels at full load: (a) DI configuration; (b) PFI configuration

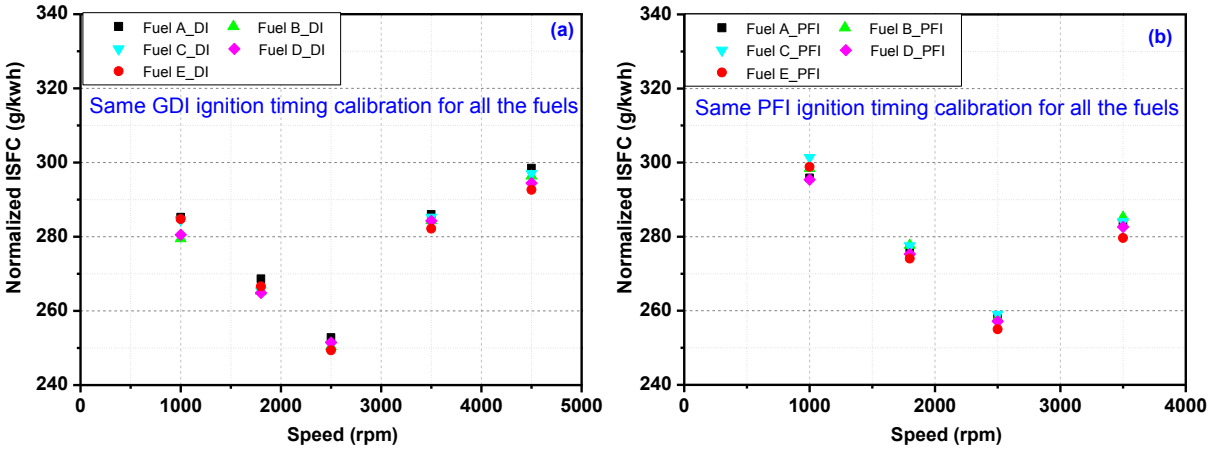

Figure 10: Normalized ISFC of all fuels at full load: (a) DI configuration; (b) PFI configuration

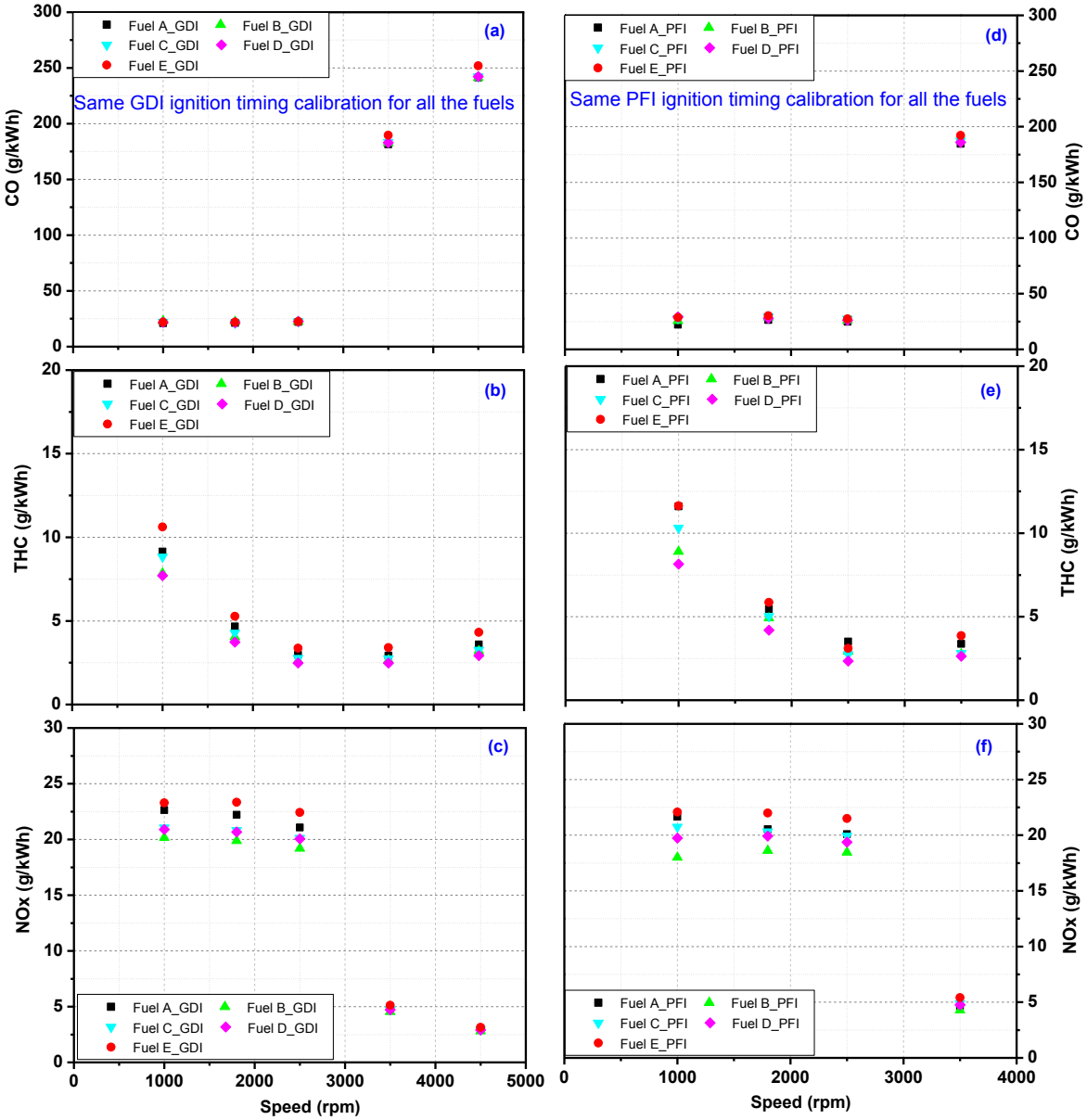

Figure 11: Gaseous emissions of all fuels at full load: (a, b and c) DI configuration; (d, e and f) PFI configuration

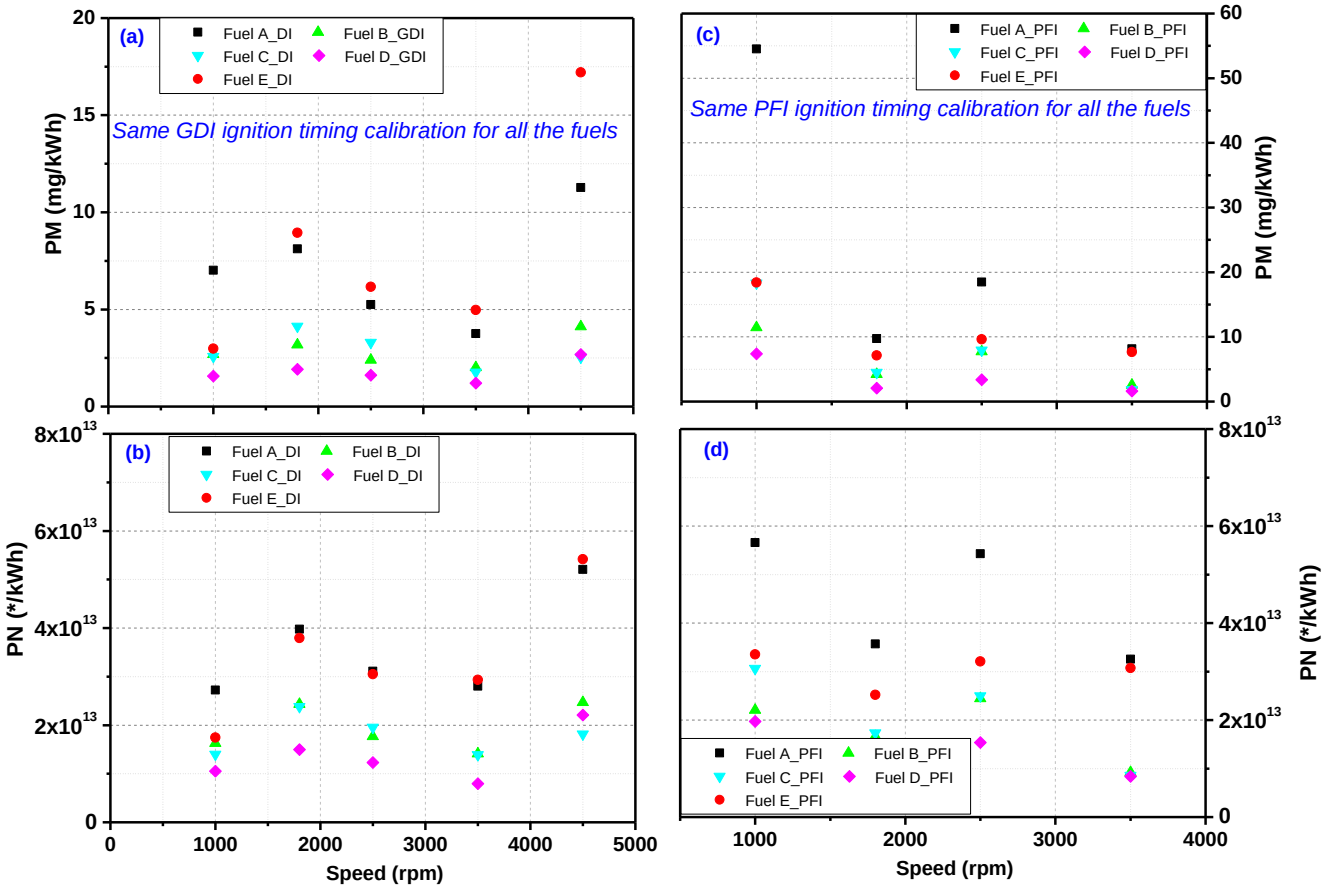

Figure 12: Particulate emissions of all fuels at full load: (a and b) DI configuration; (c and d) PFI configuration

DEFINITIONS, ACRONYMS AND ABBREVIATIONS

AFR	Air Fuel Ratio
ATDC	After Top Dead Centre
BTDC	Before Top Dead Centre
CA	Crank Angle
CA10-90	Crank angle interval between locations of 10% and 90% cumulative heat release
CA10-50	Crank angle interval between locations of 10% and 50% cumulative heat release
CA50	Crank angle at which 50% of cumulative heat release occurs
CA50-90	Crank angle interval between locations of 50% and 90% cumulative heat release
CAD	Crank Angle Degree
CO	Carbon Monoxide
COV	Coefficient of Variation
DI	Direct Injection
EGR	Exhaust Gas Recirculation
FFT	Fast Fourier Transform
FID	Flame Ionization Detector
GTL	Gas-to-liquid
HoV	Heat of Vaporization
LHV	Low Heating Value
THC	Total Hydrocarbon
IMEP	Indicated Mean Effective Pressure
MAPO	Maximum Amplitude of Filtered and Rectified In-Cylinder Pressure Oscillation
MFB	Mass Fraction Burn
MON	Motor Octane Number
NOx	Oxides of nitrogen
PFI	Port Fuel Injection
PM	Particulate Mass
PN	Particulate Number
SI	Spark Ignition
rpm	Revolutions per Minute
RON	Research Octane Number
VVT	Variable Valve Timing

REFERENCES

[1] Fischer, Tropsch. Methanol und Synthol aus Kohlenoxyds als Motorbetreibstoff. BrennstoffChemie. 1925;6: 233-4.

[2] Shell. Publicly available website: http://www.shell.com/energy-and-innovation/natural-gas/gas-to-liquids.html. 2015.

[3] Shell. GTL Fuel - Synthetic Technology for Cleaner Air, The first edition is available on the website: http://www.cpt-uk.org/_uploads/attachment/3714.pdf. Shell Knowledge Guide. 2016.

[4] Uchida N, Hirabayashi H, Sakata I, Kitano K, Yoshida H, Okabe N. Diesel Engine Emissions and Performance Optimization for Neat GTL Fuel. SAE Int J Fuels Lubr 2008-01-1405. 2008;1:748-62.

[5] Nishiumi R, Nakajima T, Kitano K, Sakata I, Clark RH. Improvement of DI Diesel Engine System by Utilizing GTL Fuels Characteristics. SAE International 2009-01-1933 ; 2009.

[6] Sajjad H, Masjuki HH, Varman M, Khan MMR, Arbab MI, Imtenan S, et al. Comparative Study of Biodiesel, GTL Fuel and Their Blends in Context of Engine Performance and Exhaust Emission. Procedia Engineering. 2014;90:466-71.

[7] Kitano K, Sakata I, Clark R. Effects of GTL fuel properties on DI diesel combustion. SAE Technical Paper 2005-01-3763; 2005.
[8] Hassaneen A, Munack A, Ruschel Y, Schroeder O, Krahl J. Fuel economy and emission characteristics of Gas-to-Liquid (GTL) and Rapeseed Methyl Ester (RME) as alternative fuels for diesel engines. Fuel. 2012;97:125-30.
[9] Clark R, Virrels I, Maillard C, Schmidt M. The performance of Diesel fuel manufactured by Shell GtL technology in the latest technology vehicles. Proceedings of 3rd Int Colloquium,"Fuels," Tech Akad Esslingen, Ostfildern, Germany Jan2001. p. 17-8.
[10] Verbeek R. Assessment of pollutant emissions with GTL as a drop in fuel for medium and heavy-duty vehicles, inland shipping and non-road machines-Final. TNO; 2014.
[11] Clark R, Battersby N, Louis J, Palmer A, Stradling R, Whale G. The environmental benefits of Shell GTL diesel. 4th International Colloquium, Esslingen, Germany. 2003.
[12] Clark R, Unsworth J. The performance of Diesel Fuel manufactured by the Shell Middle Synthesis process. 2nd International Colloquium, Esslingen, Germany. 1999.
[13] Clark R, Lampreia I, Stadling R, Wardle R. Emissions performance of Shell GTL Fuel in the future world markets. 6nd International Colloquium, Esslingen, Germany. 2007.
[14] Clark R, Stephenson T, Wardle R. Emissions measurements of Shell GTL Fuel in the context of on-road trials and laboratory studies. 7nd International Colloquium, Esslingen, Germany. 2009.
[15] Lacey P, Kientz JM, Gail S, Milovanovic N, Stevenson P, Stradling R, et al. Evaluation of Fischer-Tropsch fuel performance in advanced diesel common rail FIE. SAE Technical Paper 2010-01-2191; 2010.
[16] Leach B, Pearson R, Ali R, Williams J. CO_2 Emission Reduction Synergies of Advanced Engine Design and Fuel Octane Number. SAE Technical Paper 2014-01-2610; 2014.
[17] Stein RA, Polovina D, Roth K, Foster M, Lynskey M, Whiting T, et al. Effect of Heat of Vaporization, Chemical Octane, and Sensitivity on Knock Limit for Ethanol - Gasoline Blends. SAE Int J Fuels Lubr 2012-01-1277. 2012;5:823-43.
[18] Anderson J, DiCicco D, Ginder J, Kramer U, Leone T, Raney-Pablo H, et al. High octane number ethanol–gasoline blends: Quantifying the potential benefits in the United States. Fuel. 2012;97:585-94.
[19] Okada Y, Miyashita S, Izumi Y, Hayakawa Y. Study of low-speed pre-ignition in boosted spark ignition engine. SAE International Journal of Engines. 2014;7:584-94.
[20] Xiaofeng G, Stone R, Hudson C, Bradbury I. The detection and quantification of knock in spark ignition engines. SAE Technical Paper 932759; 1993.
[21] Baral B, Raine R. Knock in a spark ignition engine fuelled with gasoline-kerosene blends. SAE Technical Paper 2008-01-2417; 2008.
[22] Andreae MM, Cheng WK, Kenney T, Yang J. On HCCI engine knock. SAE Technical Paper 2007-01-1858; 2007.
[23] Eng JA. Characterization of pressure waves in HCCI combustion. SAE Technical Paper 2002-01-2859; 2002.
[24] Hudson C, Gao X, Stone R. Knock measurement for fuel evaluation in spark ignition engines. Fuel. 2001;80:395-407.
[25] Bradley D, Head R. Engine autoignition: The relationship between octane numbers and autoignition delay times. Combustion and flame. 2006;147:171-84.
[26] Galloni E. Dynamic knock detection and quantification in a spark ignition engine by means of a pressure based method. Energy Conversion and Management. 2012;64:256-62.
[27] Wallner T. Correlation Between Speciated Hydrocarbon Emissions and Flame Ionization Detector Response for Gasoline/Alcohol Blends. J Eng Gas Turb Power. 2011;133.
[28] Price P, Twiney B, Stone R, Kar K, Walmsley H. Particulate and Hydrocarbon Emissions from a Spray Guided Direct Injection Spark Ignition Engine with Oxygenate Fuel Blends. SAE International 2007-01-0472; 2007.

[29] Chen LF, Braisher M, Crossley A, Stone R. The Influence of Ethanol Blends on Particulate Matter Emissions from Gasoline Direct Injection Engines. SAE International 2010-01-0793; 2010.
[30] Chan TW, Meloche E, Kubsh J, Brezny R, Rosenblatt D, Rideout G. Impact of Ambient Temperature on Gaseous and Particle Emissions from a Direct Injection Gasoline Vehicle and its Implications on Particle Filtration. SAE Int J Fuels Lubr 2013-01-0527. 2013;6.
[31] Chen L, Stone R, Richardson D. A study of mixture preparation and PM emissions using a direct injection engine fuelled with stoichiometric gasoline/ethanol blends. Fuel. 2012;96:120-30.
[32] Storch M, Zigan L, Wensing M, Will S. Systematic Investigation of the Influence of Ethanol Blending on Sooting Combustion in DISI Engines Using High-Speed Imaging and LII. SAE International 2014-01-2617; 2014.
[33] Stein RA, Anderson JE, Wallington TJ. An Overview of the Effects of Ethanol-Gasoline Blends on SI Engine Performance, Fuel Efficiency, and Emissions. SAE Int J Engines 2013-01-1635. 2013;6:470-87.
[34] Vuk C, Vander Griend SJ. Fuel Property Effects on Particulates In Spark Ignition Engines. SAE International 2013-01-1124; 2013.
[35] Karavalakis G, Short D, Chen V, Espinoza C, Berte T, Durbin T, et al. Evaluating Particulate Emissions from a Flexible Fuel Vehicle with Direct Injection when Operated on Ethanol and Iso-butanol Blends. SAE International 2014-01-2768; 2014.